doi:10.1016/j.jmb.2008.04.027 J. Mol. Biol. (2008) 379, 1063–1074

JMB

Available online at www.sciencedirect.com

ScienceDirect

ELSEVIER

Structure of the Dissimilatory Sulfite Reductase from the Hyperthermophilic Archaeon *Archaeoglobus fulgidus*

Alexander Schiffer[1,2], Kristian Parey[1,2], Eberhard Warkentin[2], Kay Diederichs[1], Harald Huber[3], Karl O. Stetter[3], Peter M. H. Kroneck[1]* and Ulrich Ermler[2]*

[1]*Fachbereich Biologie, Mathematisch-Naturwissenschaftliche Sektion, Universität Konstanz, D-78457 Konstanz, Germany*

[2]*Max-Planck-Institut für Biophysik, Max-von-Laue-Str. 3, D-60438 Frankfurt, Germany*

[3]*Institut für Mikrobiologie und Archaeenzentrum, Universität Regensburg, Universitätsstraße 31, D-93053 Regensburg, Germany*

Received 7 February 2008; received in revised form 3 April 2008; accepted 10 April 2008
Available online 20 May 2008

Conservation of energy based on the reduction of sulfate is of fundamental importance for the biogeochemical sulfur cycle. A key enzyme of this ancient anaerobic process is the dissimilatory sulfite reductase (dSir), which catalyzes the six-electron reduction of sulfite to hydrogen sulfide under participation of a unique magnetically coupled siroheme–[4Fe–4S] center. We determined the crystal structure of the enzyme from the sulfate-reducing archaeon *Archaeoglobus fulgidus* at 2-Å resolution and compared it with that of the phylogenetically related assimilatory Sir (aSir). dSir is organized as a heterotetrameric $(\alpha\beta)_2$ complex composed of two catalytically independent $\alpha\beta$ heterodimers. In contrast, aSir is a monomeric protein built of two fused modules that are structurally related to subunits α and β except for a ferredoxin domain inserted only into the subunits of dSir. The [4Fe–4S] cluster of this ferredoxin domain is considered as the terminal redox site of the electron transfer pathway to the siroheme–[4Fe–4S] center in dSir. While aSir binds one siroheme–[4Fe–4S] center, dSir harbors two of them within each $\alpha\beta$ heterodimer. Surprisingly, only one siroheme–[4Fe–4S] center in each $\alpha\beta$ heterodimer is catalytically active, whereas access to the second one is blocked by a tryptophan residue. The spatial proximity of the functional and structural siroheme–[4Fe–4S] centers suggests that the catalytic activity at one active site was optimized during evolution at the expense of the enzymatic competence of the other. The sulfite binding mode and presumably the mechanism of sulfite reduction appear to be largely conserved between dSir and aSir. In addition, a scenario for the evolution of Sirs is proposed.

Keywords: dissimilatory sulfate reduction; sulfite reductase; siroheme; molecular evolution

Edited by M. Guss

Introduction

The biogeochemical sulfur cycle includes reactions between sulfur compounds in oxidation states +VI to −II, predominantly between sulfate, elemental sulfur, and hydrogen sulfide. It evolved in an early stage of prokaryotic life about 3.5 billion years ago in hot and anoxic environments.[1] Billions of tons of sulfur compounds per year are metabolized by various microbial species that use inorganic sulfur compounds as terminal electron donors or acceptors for the purpose of energy conservation. In these dissimilatory processes, specific microorganisms reduce sulfate to hydrogen sulfide under anoxic conditions and others oxidize sulfur compounds to sulfate under oxic conditions.[2,3] The biochemical pathway of dissimilatory sulfate reduction[4–7] proceeds by activating sulfate ($E^{\circ\prime} = -516$ mV)[8] to adenosine-5′-phosphosulfate ($E^{\circ\prime} = -60$ mV)[8] by ATP sulfurylase at the expense of ATP. Subsequently, adenosine-5′-

*Corresponding authors. E-mail addresses: peter.kroneck@uni-konstanz.de; ulrich.ermler@mpibp-frankfurt.mpg.de.

Present address: A. Schiffer, Department of Chemical and Analytical Sciences/Structural Biology, Sanofi-Aventis Deutschland GmbH, Industrial Park Hoechst, D-65926 Frankfurt, Germany.

Abbreviations used: Sir, sulfite reductase; dSir, dissimilatory sulfite reductase; aSir, assimilatory sulfite reductase; SirHP, aSir hemoprotein of *Escherichia coli*.

phosphosulfate is hydrolyzed and reduced to sulfite and AMP by adenosine-5′-phosphosulfate reductase, and the generated sulfite is finally reduced to hydrogen sulfide by sulfite reductase (Sir) in a six-electron transfer process[8]:

$$HSO_3^- + 6e^- + 6H^+ \rightleftarrows HS^- + 3\ H_2O$$
$$E^{\circ\prime}(HSO_3^-/HS^-) = -116\ \text{mV}$$

In sulfur-oxidizing organisms, this pathway proceeds in the opposite direction starting from hydrogen sulfide, elemental sulfur, or thiosulfate.[9] In contrast, assimilatory reduction of sulfate is achieved by a wide variety of organisms of all three domains of life (but not of animals) and provides the cell with sulfur in oxidation state −II, which is vital for biosynthesis of sulfur-containing amino acids and cofactors.[10,11] The latter process deviates in some organisms from the dissimilatory pathway as adenosine-5′-phosphosulfate is first phosphorylated by adenosine-5′-phosphosulfate kinase and reduced by phosphoadenosine-5′-phosphosulfate reductase, which is distantly related to adenosine-5′-phosphosulfate reductase.[12]

Sirs are considered as the key enzymes in both the assimilatory and dissimilatory metabolism of sulfur. They diverged according to sequence analysis studies from a common ancestor into four groups prior to the bacterial/archaeal divergence[13,14]: the monomeric assimilatory Sir (aSir),[15] the low-molecular-weight aSir,[16] the dissimilatory Sir (dSir; working in both reductive and oxidative directions),[9] and a special dSir found in a few anaerobic bacteria only.[17] Notably, assimilatory nitrite reductases, which convert nitrite to ammonia, also belong to the Sir family.[18]

dSirs have been isolated from several sulfate-reducing microorganisms, such as *Desulfovibrio vulgaris*,[19] *Desulfovibrio desulfuricans*,[20] *Pyrobaculum islandicum*,[21] and *Archaeoglobus fulgidus*,[22] and have been characterized with respect to their molecular, spectroscopic, and kinetic properties. The dSirs studied so far are composed of a heterotetrameric $(\alpha\beta)_2$ core complex and, depending on the organism, two additional small subunits, γ and δ, resulting in an $(\alpha\beta)_2\gamma_n\delta_n$ multisubunit complex.[23] The subunits α, β, γ, and δ have molecular masses of approximately 45, 43, 10, and 11 kDa, respectively, with subunits α and β being related with respect to their primary sequence. The $(\alpha\beta)_2$ core complex harbors the coupled siroheme–[4Fe–4S] center as well as [4Fe–4S] clusters. The published cofactor stoichiometries range from two to four sirohemes and three to six [4Fe–4S] clusters per $(\alpha\beta)_2$ heterotetramer, depending on the organism and the purification procedure applied.[13] Perhaps the most intriguing spectroscopic property of Sir results from the presence of a set of complex EPR signals assigned to high-spin $S = 5/2$ and $S = 9/2$ iron–sulfur centers.[24] The $S = 5/2$ resonances were present in both aSirs and dSirs,[24–28] whereas the $S = 9/2$ signals were observed in several dSirs only, including *D. vulgaris*[24] and *A. fulgidus*.[7,28]

Sir activity can be clearly linked to the $(\alpha\beta)_2$ core complex, while the functions of the small subunits γ and δ remain unknown so far. The γ subunit carries a redox-active disulfide bond that might function in electron transfer to an external electron donor so far not identified.[29] Subunit δ is characterized by a winged-helix motif, suggesting a role in DNA binding and regulation.[30] While the $(\alpha\beta)_2$ core complex of dSir has not been structurally characterized so far, a few crystal structures have been reported for aSirs and related enzymes, such as the *Escherichia coli* hemoprotein in a truncated form[31] and subsequently the *Mycobacterium tuberculosis* enzyme[32] and the spinach nitrite reductase.[33] A characteristic structural feature of the enzymes of the Sir family is their trilobal architecture. Lobes 1 and 2 (solely found in Sir) are composed of a mixed β-sheet flanked by α-helices, and lobe 3 is built by two attached ferredoxin-like domains. In the central intersecting points of the three lobes resides a siroheme center bridged to a [4Fe–4S] cluster via a cysteine thiolate, forming a unique electronically coupled multimetal center.[31]

In this report, we present the crystal structure of the dSir $(\alpha\beta)_2$ core complex isolated from the hyperthermophile *A. fulgidus* at 2.0-Å resolution. Although this organism has been shown to be of ancient origin,[34] its Sir resulted from a lateral gene transfer event from a deeply branched bacterial lineage,[35,36] indicating nevertheless a slow rate of development and therefore an archaic nature of dSir. The structures of dSir and aSir are compared with regard to their overall architecture, arrangement of metal cofactors, electron transfer processes, and evolutionary development.

Results and Discussion

The dSir of *A. fulgidus* was purified to homogeneity and crystallized under the strict exclusion of dioxygen. The specific activity of 48.2 nmol sulfite min^{-1} mg^{-1} was in the same range as that reported for dSir from various sulfate-reducing bacteria.[19,20,37] The diffraction data were phased with the MAD/SIRAS method using intrinsic iron atoms and a mercury derivative (Table 1). Structural refinement converged to R and R_{free} values of 18.9% and 22.4%, respectively, in the resolution range of 10.0–2.0 Å. The asymmetric unit contained one $(\alpha\beta)_2$ heterotetramer (Fig. 1). One αβ dimer shows a well-shaped electron density, and the structural analysis is mainly based on its data, whereas the density of the second αβ dimer is much less defined, in some loop regions even disordered. The folds of the αβ heterodimer of dSir are related to those of aSir and spinach nitrite reductase,[31–33] but both subunits additionally contain an inserted ferredoxin domain (Figs. 1 and 2b). The structures of dSir and aSir reveal both a high degree of relationship and interesting differences that are discussed in the following. For comparative studies between aSir and dSir, we preferentially use the aSir hemoprotein of *E. coli* (called SirHP hereafter) because of its highly resolved X-ray structure.[31]

Table 1. Data statistics

	Native	Hg[a] peak	Hg[a] inflection	Fe[a] peak	Fe[a] inflection	Hg/Fe[a] remote
Data collection						
Wavelength (Å)	0.9393	1.0	1.009	1.733	1.742	0.95
Resolution range (Å)	30.0–2.0 (2.16–2.0)	40.0–2.7 (2.9–2.7)	40.3–3.1 (3.2–3.1)	40.0–2.9 (3.1–3.0)	40.0–3.1 (3.2–3.1)	40.0–3.1 (3.2–3.1)
Space group	$P2_1$	$P2_1$	$P2_1$	$P2_1$	$P2_1$	$P2_1$
Completeness (%)	95.3 (79.4)	99.7 (99.9)	77.5 (79.5)	93.9 (99.7)	83.5 (84.5)	97.1 (98.7)
R_{sym} (%)	8.7 (39.1)	9.9 (43.8)	12.6 (60.9)	13.3 (49.7)	18.2 (67.9)	15.1 (57.2)
$I/\sigma(I)$	7.4 (2.3)	9.5 (2.9)	10.2 (2.3)	8.9 (2.4)	7.5 (1.7)	8.6 (2.0)
Redundancy	2.5 (2.4)	3.1 (3.1)	2.7 (2.9)	3.0 (2.9)	2.5 (2.3)	2.7 (2.5)
Wilson *B*-value (Å^2)	24.8 (25.3)					
Refinement statistics						
No. of residues, sirohemes, [4Fe–4S] clusters, and solvent molecules	1560, 4, 8, 342					
No. of molecules in a.u.	1					
Resolution range (Å)	20.0–2.0 (2.05–2.0)					
Reflections ($F>0\sigma$)	108,315					
$R_{working}$, R_{free} (%)	18.9, 22.4 (27.1, 32.0)					
B-value (Å^2) α_1, β_1, α_2, β_2	28.4, 21.4, 69.0, 74.0					
Bond-length deviation (Å)	0.018					
Bond-angle deviation (°)	1.86					

[a] The MAD/SIRAS data set was collected with one crystal that was soaked for 1 h in the reservoir solution + 0.05 mM thimerosal.

Oligomeric states

The characteristic trilobal architecture of Sir is realized in dSir by a heterodimer composed of tightly associated subunits α and β (called dSir-α and dSir-β), and not by a monomer as in aSirs and assimilatory nitrite reductases (Figs. 1 and 2). In aSir, equivalent parts of dSir-α and dSir-β have been fused into a single chain, by means of a 40-Å-long linker segment that wraps around the molecule.[31] Both dSir-α and dSir-β, and their equivalent moieties in aSir called aSir-a (or SirHP-a) and aSir-b (or SirHP-b), respectively, are related by the same pseudo-2-fold symmetry axis. This is documented by an rms value of 3.3 Å (88% of the residues) between dSir and SirHP, compared with that of 2.4 Å (89%) between dSir-α

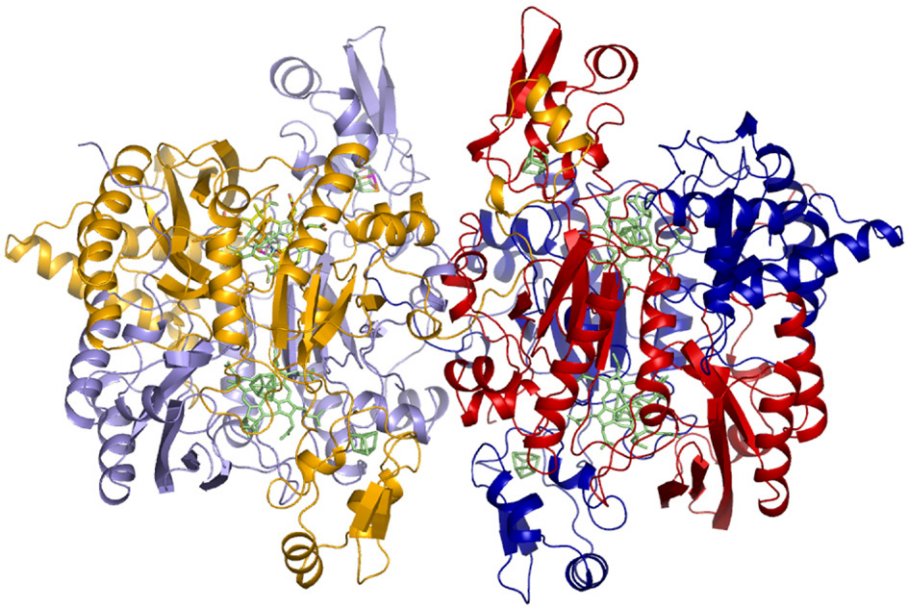

Fig. 1. Structure of the dSir of *A. fulgidus* organized as an $(\alpha\beta)_2$ heterotetramer with a size of 125 Å × 80 Å × 60 Å. The heterotetramer is built of two attached αβ units (α subunits are shown in orange and red; β subunits, in light blue and dark blue). The C-terminal arms of both subunits are major constituents of their interface. The cofactors are shown as a stick model in green.

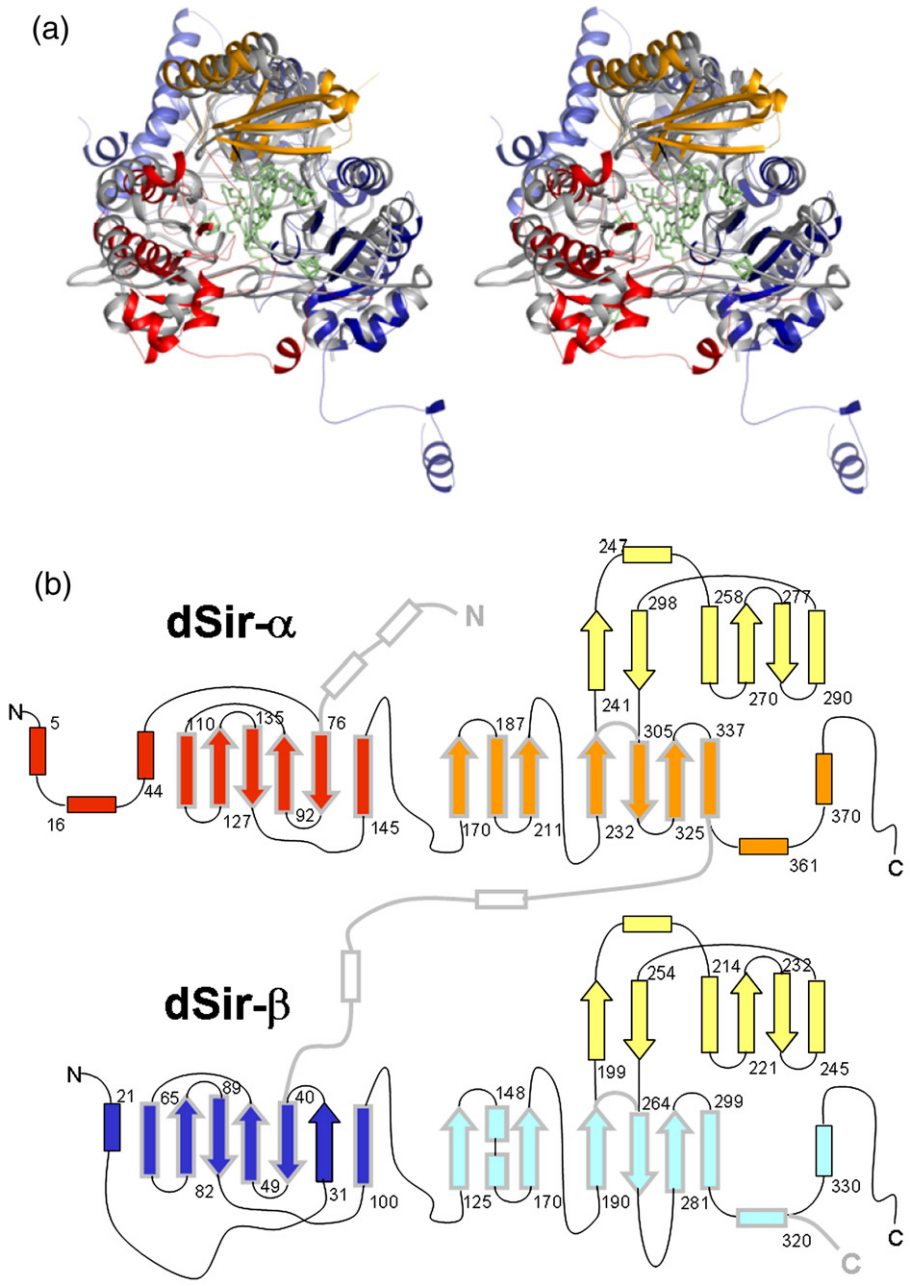

Fig. 2. Architecture of Sir. (a) Stereoview of dSir and complete aSir from *M. tuberculosis* superimposed. The trilobal structure is realized in dSir by an αβ heterodimer and in aSirs (shown in gray) by a monomer. Lobe 1 (in red) is composed of residues α165–α416; lobe 2 (in blue), β120–β366; and lobe 3 (in orange and light blue), the corresponding subdomains α70–α160 and β30–β115. For clarity, both inserted ferredoxin domains were omitted. (b) Schematic representation of the fold of subunits α and β using the same colors. The inserted ferredoxin domains are shown in yellow. The fold of aSir is marked as light gray margins.

and SirHP-a and that of 4.0 Å (89%) between dSir-β and SirHP-b.[38] Interestingly, both dSir-α and dSir-β exhibit higher structural similarities to aSir-a than to aSir-b. In line with this finding, aSir-a represents the major constituent of the siroheme binding and active site, which was consequently more conserved as aSir-b. Accordingly, dSir-α and dSir-β are structurally more related than SirHP-a and SirHP-b, as reflected in sequence identities of 25% and 16% and in rmsd values of 2.2 and 3.2 Å, using 91% and 83% of the C^{α} atoms, respectively. While the β-sheet scaffold is largely preserved in all Sirs, the calculated rms differences are clearly visible in the displacements of the surrounding helices and loop segments.

Substantial structural differences between dSir-α and dSir-β and between both and aSir are found at the N- and C-terminal ends (Figs. 1 and 2b). Both ends are involved in intradimer and interdimer interface formations (see below). Consequently, the buried surface area between dSir-α and dSir-β is larger than that between the aSir-a and aSir-b moieties of aSir, which obviously compensates for the loss of free

energy for separating the chains. The residual interface is mostly formed by equivalent segments in dSir and aSir, but the individual residues involved differ completely.

On the basis of gel filtration experiments, dSir of *A. fulgidus* was previously described as an $(\alpha\beta)_2$ heterotetrameric enzyme complex[22] (Fig. 1) that was now confirmed by the X-ray structure. The buried surface area between two αβ heterodimers of 4567 Å^2 (9.1% of the entire surface)[39] corresponds to values found for other oligomeric proteins.[40] The interface between the two αβ units is largely formed by the extended C-terminal segments of both subunits that are either wrapped around the counter heterodimer or completely encapsulated by it. The C-terminal regions are not generally preserved in dSir such that the heterotetrameric oligomeric state cannot be predicted for all family members from their primary structure. Moreover, the heterotetrameric organization of dSir does not appear to be of functional importance for the reduction of sulfite to hydrogen sulfide. The reaction proceeds most likely in an independent manner at the active sites of the two αβ units, which are about 50 Å apart from each other (Fig. 1). Hence, a tetrameric architecture of dSir might rather be a relic from its development in hot environments that was then conserved during evolution. Oligomerization is a frequently used strategy for hyperthermophilic proteins to increase their stability by reducing the surface area-to-volume ratio.[41] However, a role of the heterotetramer in the transfer of six electrons to sulfite cannot be completely excluded as the molecular basis of this process has not been established yet.

Siroheme–[4Fe–4S] center

The dissimilatory enzyme of *A. fulgidus* definitively harbors the same multimetal center composed of a siroheme ring coupled to a [4Fe–4S] cluster via a cysteine thiolate bridge, as observed in aSir. A novel feature of dSir compared with aSir results from the presence of a second siroheme–[4Fe–4S] center in each αβ heterodimer (Fig. 2a). The two centers are termed 'functional' and 'structural' in the following as the latter is catalytically not productive (see below). The presence of four siroheme–[4Fe–4S] centers plus four additional [4Fe–4S] clusters in dSir

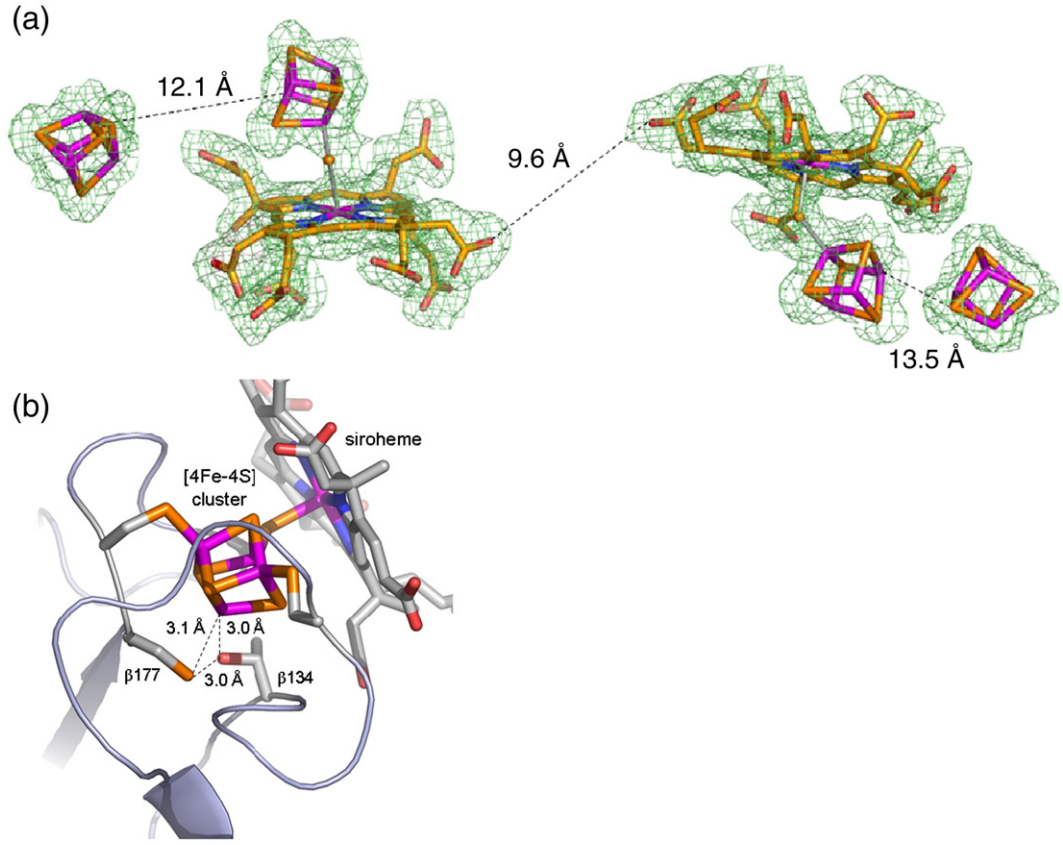

Fig. 3. Cofactors of the dSir of *A. fulgidus*. (a) Arrangement of the siroheme–[4Fe–4S] centers and the peripheral [4Fe–4S] clusters in the αβ heterodimer. The functional siroheme–[4Fe–4S] center (at the right side) is the site of sulfite reduction and most likely receives the required electrons from the adjacent peripheral [4Fe–4S] cluster. According to the vicinity of the sirohemes, the structural siroheme–[4Fe–4S] center could also serve as an electron donor for the functional center. The well-formed electron density at 2 Å is shown at a contour level of 2σ. (b) Surrounding of the fourth iron of the [4Fe–4S] cluster of the functional siroheme–Fe/S cluster. Unexpectedly, the fourth iron is not ligated by a cysteine as found for dSir-α and aSir but by a threonine (Thrβ134). Alternatively, Cysβ177 approaches the iron to about 3 Å, which is, however, too far away for coordination.

of *A. fulgidus*, and presumably in all heterotetrameric dSirs, comprising altogether 36 Fe and 32 acid-labile sulfur atoms, is compatible with conclusions from sequence comparison studies but deviates from most values determined by chemical analysis.[13]

Interestingly, the two sirohemes are in close neighborhood and are arranged in a manner that rings B and C project toward each other (Fig. 3). With a minimal distance of 9.6 Å between the acetate carboxylates of ring C, they mutually participate in forming their binding pockets and thereby rigidify and stabilize each other. Both sirohemes are multiply linked via the polypeptide scaffold, which would allow an electron transfer and perhaps weak electronic coupling between both. The most direct connection is formed between the ring C carboxylate group of both sirohemes mediated by Argα229 and a solvent molecule via hydrogen bonds.

In contrast, the site that would correspond to the missing structural siroheme–[4Fe–4S] center in aSir has become substantially rearranged. Most importantly, the linker segment between aSir-a and aSir-b occupies the position of the siroheme (Fig. 2). Other structural features, such as the modified central β-sheet of lobe 1 (i.e., devoid of the first strand) and the shortened loops 35:41, 114:130, 166:170, and 315:319 of SirHP-b compared with dSir-β, also prevent binding of the siroheme–[4Fe–4S] center (Fig. 2a). The binding site of the coupled siroheme–[4Fe–4S] cluster in aSir is abolished by restructuring the polypeptide segment carrying the [4Fe–4S] cluster and by replacing all four ligating cysteines of aSir-b, dSir-α, and dSir-β.

A comparison of the conformation and the binding mode of the functional and structural siroheme–[4Fe–4S] centers within dSir, and between dSir and aSir, revealed that the positions of the coupled centers as well as the enveloping polypeptide scaffold and its electrostatic properties are mostly preserved despite any significant overall sequence identity. Nevertheless, a few significant structural differences exist. First, the macrocyclic siroheme ring system in dSir is less ruffled than that in SirHP, which concomitantly increases the distance between the siroheme and the adjacent [4Fe–4S] cluster. The closest contact between the CHB atom of the macrocyclic ring and the S1 sulfur of the [4Fe–4S] cluster increases from 3.6 Å in SirHP to 4.3 Å in the functional center of dSir. The distortions from planarity of the functional and the structural sirohemes of dSir are similar; however, the minimal distance to the [4Fe–4S] cluster increases to 4.6 Å in the latter. Second, the conformations of the siroheme acetate and propionate substituents are substantially altered as a consequence of the number, nature, and conformation of the interacting positively charged residues (Fig. 4). Only a few positively charged residues are conserved between the functional and structural sirohemes of dSir but none is conserved between dSir and SirHP. However, several basic side chains are topologically preserved both between the functional and structural sirohemes of dSir and between those of SirHP and dSir (Fig. 4). It is conceivable that specific conformations of the basic residues will induce the pronounced saddle-shaped distortion of the siroheme ring in SirHP. A third difference is related to the binding mode of the [4Fe–4S] cluster bridged to the functional siroheme moiety despite the high degree of conservation. Only three of the four iron atoms of dSir are ligated to the invariant thiolate groups of Cysβ140, Cysβ182, and Cysβ178 with distances between 2.2 and 2.4 Å. The fourth iron atom forms a polar contact to the hydroxyl group of Thrβ134 (replaces the ligating cysteine in aSir) and to the thiol group of Cysβ177 (Fig. 3b). Cysβ177 is replaced by a glycine in dSir-α and in aSir. However, the distances of ca 3 Å between the iron and the side chain oxygen of Thrβ134 and the sulfur of Cysβ177, respectively, argue against a direct ligation. This is astonishing as small conformational changes would place the thiol sulfur in a ligating position.

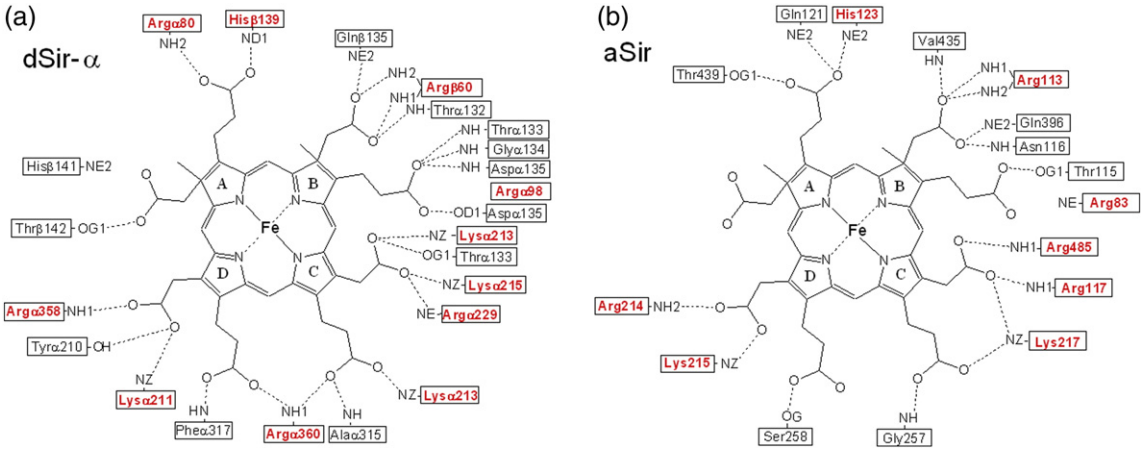

Fig. 4. Interactions between the polypeptide and the siroheme–Fe/S centers in dSir-α (a) and SirHP (b). The sirohemes are embedded into a positively charged pocket compensating for the negative charge of eight carboxylate groups. However, the conformation of the propionate and acetate groups and that of the contacting basic residues (highlighted in red) are not conserved between dSir and aSir. The functional siroheme of dSir interacts directly with 11 basic residues; the siroheme of SirHP, with 8.

Catalytic reaction

Although each of the αβ heterodimers harbors two complete sets of siroheme–[4Fe–4S] centers to catalyze the six-electron reduction of sulfite to hydrogen sulfide, a sulfite binding site is only formed in front of the *si*-side of one (the functional) siroheme center (Fig. 5). The substrate binding site is located at the end of an ~15-Å-long funnel formed by the inserted ferredoxin domain as well as lobes 1 and 3 of dSir-α (Fig. 5a). Based on available structural information,[31–33] the siroheme center and the sulfite binding site appear to be more deeply buried in dSir than in aSir. This finding might change when the natural electron donors bind to aSirs. Nevertheless, the substrate binding site is more shielded in aSir mainly due to the covalently linked Tyr69–Cys161 pair and Arg64 in *M. tuberculosis* aSir and due to Lys91, Phe96, and Met175 in spinach nitrite reductase. Note that these segments are partly truncated in SirHP. In contrast, the potential substrate binding site in front of the structural siroheme center is covered by a β-bulge that is formed by prolonging the loop preceding strand β126:β134 (Fig. 5b). The side chain of Trpβ119 is directed from the β-bulge toward the *si*-side of the siroheme and thus completely prevents sulfite binding. The tryptophan residue at position 119 is not strictly preserved but conservatively exchanged frequently by a phenylalanine. Additionally, catalytically important amino acid residues (present in front of the functional siroheme; see below) are essentially substituted and the negatively charged acetate and propionate groups of rings A and D point toward the *si*-side of the structural siroheme and thus repel incoming anions (Fig. 5b).

The prevention of catalysis at the structural siroheme–[4Fe–4S] center might be driven by the benefit of the enzyme to contain one optimized, highly productive active site as opposed to two less efficient active sites. Due to the close proximity of the two coupled siroheme–[4Fe–4S] centers, optimization at one active site automatically requires conformational changes at the other. The functional siroheme–[4Fe–4S] center and the sulfite binding site might be adjusted by rigidifying the binding site of the structural siroheme–[4Fe–4S] center, which is supported by its lower temperature factor (5 $Å^2$) compared with that of the functional center. From an economical point of view, the synthesis of a siroheme–[4Fe–4S] center to stabilize the active site of the enzyme appears fairly expensive. Therefore, dSir has to be regarded as an intermediate suboptimal solution of the evolutionary process that was overcome during the evolution of aSirs. Usage of cofactors for structural reasons is rare in enzymes but not unprecedented.[42] Note also that a functional role of the structural siroheme–[4Fe–4S] center in the electron transfer process cannot be ruled out.

The assignment of the substrate binding site at the functional siroheme is supported by the presence of a bulky electron density at the position of the distal ligand although the nature of the ligand remains unclear. The electron density shape certainly does not match to a sulfite or a phosphate ion. Compared with the structural siroheme center where the iron atom is placed toward the *re*-face of the ring plane, the iron atom of the functional siroheme moiety sits in the plane center and coordinates with the distal ligand. Accordingly, the distance values between the bridging thiolate sulfur of Cysα223 and that of Cysβ182 and the iron atom of the structural and functional centers are 2.5 and 2.8 Å, respectively. The latter value corresponds to that found in SirHP.

The yet unidentified distal ligand at the functional siroheme is embedded into a positively charged pocket (Fig. 5a) mainly formed by side chains of Argα98, Argα170, Lysα211, Lysα213, Thrα133, and four firmly bound solvent molecules around them. The four positively charged residues are strictly conserved in dSirs and aSirs, and their long side

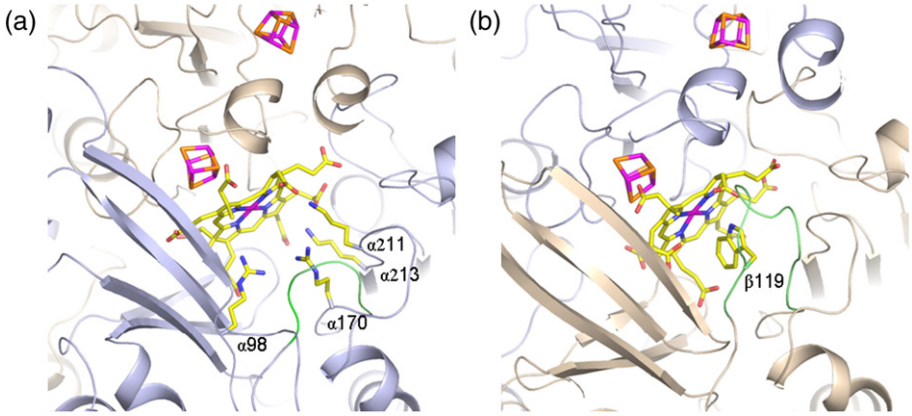

Fig. 5. Potential sulfite binding site. (a) At the functional siroheme–[4Fe–4S] center, the four key residues Argα98, Argα170, Lysα211, and Lysα213 conserved in aSir and dSir constitute the pocket for binding sulfite and contribute significantly to catalysis. (b) At the structural siroheme–[4Fe–4S] center, the sulfite binding is blocked by a prolonged loop (in green) preceding strand β126:β134, from which the bulky side chain of Trpβ119 occupies the position of the substrate in front of the siroheme iron. For comparison, the equivalent loop in front of the functional siroheme–[4Fe–4S] center is also marked in green.

chains adopt highly similar conformations and positions emphasizing their catalytic importance. Thrα133, which is only conserved in dSirs, becomes replaced in aSirs by an arginine that points away from the sulfite. Due to the nearly identical designs of the sulfite binding pocket in aSir and dSir, we assume similar mechanisms for the destabilization of the S–O bond of sulfite and its protonation, which is described in detail for aSir.[31]

Our structural data of dSir from *A. fulgidus* clearly document that the sequence "C–X_5–C–n–C–X_3–C" represents an insufficient recognition motif for Sirs as it only recognizes the siroheme–[4Fe–4S] center. Actually, it solely identifies the [4Fe–4S] cluster, and not the sulfite binding site and the catalytically important amino acid residues. A conserved stretch involved in sulfite binding helps define a second recognition sequence, "p–Y–K–a–K–s–K" (a, aliphatic; s, small), for dSirs containing the two invariant lysines mentioned above. An analogous fingerprint "P–R–K–a–K–a–s" can be defined for aSirs, whereby the "K–a–K" motif is shared by dSirs and aSirs. Notably, the recognition sequence contains at position 2 in dSir a tyrosine and in aSir an arginine, both pointing to the ring D acetate. This might contribute to the different ring ruffling found in SirHP and dSir. The equivalent fingerprint "P–R–K–a–N–a–s" for assimilatory nitrite reductase resembles that for aSir except for the exchange of lysine by asparagine in position 5, as reported previously.[31]

Electron delivery

Sirs are coupled to different electron delivery systems to reduce/oxidize the siroheme–Fe/S center. While, for example, NADPH supplies reducing equivalents to eight flavoprotein subunits linked to four SirHP subunits in *E. coli* aSir,[43] transiently bound ferredoxins donate the electrons, one by one, to sulfite in *M. tuberculosis* aSir and in spinach nitrite reductases.[44] In dSir, the molecular components of the electron transfer machinery have not been identified so far.

In contrast to aSir, however, both dSir-α and dSir-β have inserted an extra domain with a classical bacterial ferredoxin fold harboring a [4Fe–4S] cluster. The X-ray structure suggests that these so-called peripheral [4Fe–4S] clusters might serve as intermediate electron carriers between an unknown external electron donor and the siroheme–Fe/S center (Fig. 3). According to the DALI software,[38] the inserted domain is most closely related to the ferredoxin domain of adenosine-5′-phosphosulfate reductase,[45] the preceding enzyme in the dissimilatory sulfate reduction pathway. The two peripheral [4Fe–4S] clusters of the ferredoxin domains are embedded into a hydrophobic pocket, and the four iron atoms are respectively ligated to the thiol groups of Cysβ220, Cysβ241, Cysβ244, and Cysβ247 and to the thiol groups of Cysα266, Cysα286, Cysα288, and Cysα291. The closest distances from the peripheral [4Fe–4S] clusters to the functional and structural siroheme–[4Fe–4S] centers are 13.5 and 12.1 Å, respectively (Fig. 3), which are in the right range to shuttle electrons at physiological rates.[46] The most direct electron transfer pathway to the functional siroheme–[4Fe–4S] center extends from Cysβ178 to Cysβ244 (ligands of the functional center and the peripheral [4Fe–4S] cluster of dSir-β) via a tightly bound solvent molecule that interacts with their thiol and main chain carbonyl groups, respectively. In comparison, the shortest link to the structural siroheme–[4Fe–4S] center is provided via Metα289, whose side chain interacts with the thiol group of Cysα219 of the structural center and whose peptide amine nitrogen contacts a sulfur of the peripheral [4Fe–4S] cluster. Thus, a rapid electron transfer is geometrically feasible between both the functional and structural siroheme–[4Fe–4S] centers and their adjacent peripheral [4Fe–4S] cluster. The latter [4Fe–4S] cluster might also channel electrons to sulfite via the structural and functional siroheme–[4Fe–4S] centers (Fig. 3).

According to our current knowledge about the energy metabolism of *A. fulgidus* and other sulfate reducers, the electrons originate from a quinol pool in the cell membrane that is generated by oxidizing organic substrates, such as lactate.[47] The thereby reduced coenzyme F_{420} is subsequently oxidized, and the quinone is reduced by a proton-translocating $F_{420}H_2$ menaquinone oxidoreductase.[48] Finally, the generated quinol is oxidized by the membrane protein complex Hme[49] and the electrons are transferred to Sir by a yet unknown pathway. One could speculate that the reducing equivalents are transferred via thiol/disulfide couples from this protein complex to the peripheral [4Fe–4S] cluster of dSir as Hme is phylogenetically related to a heterodisulfide-reducing enzyme[50] and subunit γ, which is strongly associated to various dSirs, contains a redox-active disulfide bridge.[29] Although the complex between the $(\alpha\beta)_2$ core and subunit γ has not been structurally characterized, docking experiments clearly indicate that the peripheral [4Fe–4S] cluster of the inserted ferredoxin and the redox-active thiol/disulfide couple of subunit γ can be positioned in sufficiently close distance to allow rapid electron transfer.[46] Interestingly, the ferredoxin domain in the vicinity of the functional siroheme–[4Fe–4S] center harbors a disulfide bridge adjacent to the protein surface, 8 Å apart from the peripheral [4Fe–4S] cluster. However, an essential role in the electron transfer process remains questionable since Cys211 and Cys251 are mostly but not strictly conserved. Further biochemical studies will be unquestionably required to identify and characterize the missing electron-transferring components and to fully understand the electron-supplying machinery of sulfate reduction. Finally, the structural analysis of dSir and aSir revealed only minor differences in the active sites for sulfite reduction. It is therefore possible that an efficient supply of electrons in a controlled and specific manner might also be an important factor to explain mechanistic differences among the various members of the Sir family.

Molecular evolution

Sirs have evolved over a period of about 3.5 billion years with different rates and under different environmental pressure and physiological constraints. Comparative studies reveal that the basic structural framework, including the unique electronically coupled siroheme–[4Fe–4S] center and most likely the mechanism of the six-electron reduction of sulfite, has been remarkably conserved. On the other hand, the oligomeric state, the degree of internal structural relationships, the number of prosthetic groups, and the electron delivery system differ between dSir and aSir. These observations prompted us to propose a scenario of protein evolution as depicted in Fig. 6.

It starts with the fusion of a larger α/β domain carrying a [4Fe–4S] cluster (lobe 1) and a smaller α/β domain (the first moiety of lobe 3). This new monomer has to be furnished (accidentally) with surface properties that will allow weak interactions with a siroheme molecule and with a second monomer in such a manner that the [4Fe–4S] cluster of one monomer faces the siroheme moiety of the other (Fig. 2a). The juxtaposition of cofactors or metals protruding from different folding units is a common theme in the evolution of cooperating cofactors, as observed, for example, in rubredoxin:NO/O_2 oxidoreductase[51] and in methanol:cobalamin methyltransferase.[52] In Sirs, the thiolate bridge between the [4Fe–4S] cluster and the siroheme iron will significantly contribute to stabilize the dimeric form. A thereby generated weak activity for reducing anions, such as nitrite and sulfite, will be enhanced by spontaneous mutation events that increase the monomer–monomer interactions and the affinity between the protein matrix and both the siroheme–[4Fe–4S] centers and inorganic ions. Up to this point, aSir and dSir are presumably not distinguishable. According to our currently limited knowledge about the oligomeric composition of the low molecular-mass-aSir[16] and the unusual dSir,[17] these two enzymes do not fit into this concept as none of them assembles in a manner that a siroheme center and a [4Fe–4S] cluster juxtapose.

Further catalytic optimization of Sir is accomplished by a gene duplication event, one of the major sources of evolutionary development.[53] This becomes evident from the strong structural relationship between dSir-α and dSir-β and between aSir-a and aSir-b. The branching point between dSir and aSir cannot be definitely derived. The high primary and tertiary structure relationship between the peripheral ferredoxin domains of dSir-α and dSir-β (33%, rms = 1.9 Å) suggests insertion prior to gene duplication of dSir and consequently separated development between aSir and dSir before this event. The absence of any overall sequence relationship between aSir-a and dSir-α despite catalyzing the same reaction and originating from a common ancestor also argues for an earlier separation as that of dSir-α and dSir-β. The missing sequence identity between aSir-a and aSir-b in contrast to dSir-α and dSir-β indicates that the molecular evolution of aSir has been subjected either to a higher rate of amino acid exchange or to an earlier gene duplication compared with dSir, with the latter possibility also arguing for branching prior to this event.

After gene duplication, the development of dSir focuses on the optimization of the active site at the functional siroheme–[4Fe–4S] center. This is accompanied by modifications in the regions of the structural siroheme–[4Fe–4S] center that concomitantly eliminate its own enzymatic competence. In parallel, tetramerization of dSir occurs as the interface formation is based on the differentiation of dSir-α and dSir-β, particularly of their C-terminal ends. Afterward, divergence of the bacterial and archaeal lineages takes place as derived from sequence comparison studies. The development of aSir might pass through a stage described for dSir but goes subsequently beyond that by fusing the two subunits and by removing the structural siroheme–[4Fe–4S] center. Both processes are coupled since the linker segment between aSir-a and aSir-b complements the abolished structural siroheme–[4Fe–4S] center.

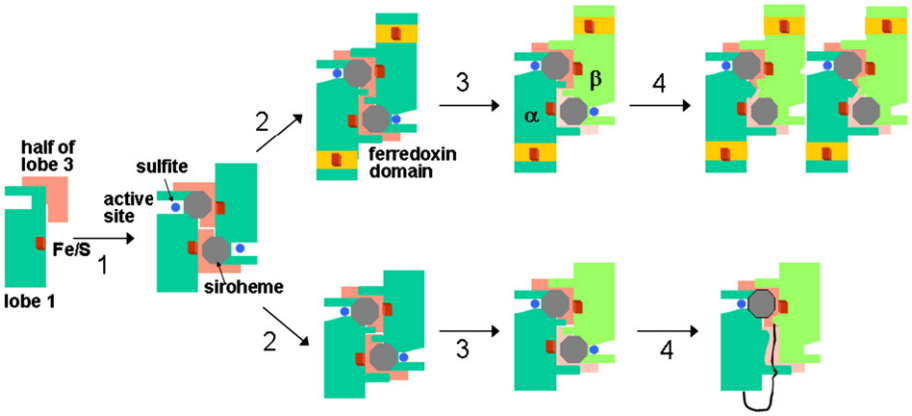

Fig. 6. Evolution of Sir. The proposed route is based on the assumption that branching between the dSirs and aSirs occurs prior to gene duplication. The following steps are illustrated: (1) dimerization; (2) optimization by spontaneous mutagenesis; (3) gene duplication; and (4) gene fusion and tetramerization.

Together with gene duplication, gene fusion is the most important force driving protein evolution.[54,55]

Materials and Methods

Purification

The cultivation of *A. fulgidus* (DSM 4304T) was carried out as previously described.[34] Frozen cells were transferred to an anaerobic chamber (95% N_2, 5% H_2; Coy) and suspended in 1–2 volumes of 20 mM potassium phosphate buffer, pH 7.0, containing a few crystals of deoxyribonuclease I and 5 mM $MgCl_2 \cdot 6H_2O$. Cells were disrupted in a French press, and the lysate was centrifuged at 100,000*g*. The soluble fraction was applied to a Q Sepharose Fast Flow column (1.6 cm × 10.0 cm; Amersham Pharmacia Biotech) equilibrated with 20 mM potassium phosphate buffer, pH 7.0. dSir eluted in a linear gradient (0–1.0 M KCl) at about 0.54 M KCl. Fractions containing dSir were combined and desalted by ultrafiltration (cutoff = 30 kDa; Amicon) with subsequent dilution with 20 mM potassium phosphate buffer, pH 7.0, and 5% (v/v) glycerol. The desalted protein was loaded onto a Resource Q15 column (1.0 cm × 13 cm; Amersham Pharmacia Biotech) and eluted by a linear gradient (0–1 M KCl) at about 0.27 M KCl. The combined fractions were concentrated by ultracentrifugation and loaded onto a Superdex™ 200 HiLoad™ 26/60 gel filtration column (2.6 cm × 60 cm; Amersham Pharmacia Biotech) equilibrated with 50 mM potassium phosphate buffer, pH 7.0, 150 mM NaCl, and 5% (v/v) glycerol. Protein was concentrated to 20 mg/ml and stored at 100 K in 100 mM Tris–HCl, pH 7.0.

Crystallization and data collection

Initial crystals were obtained with the hanging-drop method using the Hampton sparse matrix screening setup. Optimization led to a drop content of 1 μl of protein solution and 1 μl of reservoir solution composed of 20% PEG (polyethylene glycol) 4000, 0.1 M sodium citrate, 0.2 M NaCl, and 5% 2-propanol. The crystals grew in space group $P2_1$ with unit cell parameters of 94.8 Å, 69.4 Å, 148.3 Å, and 106.9°, with two α and two β subunits in the asymmetric unit ($V_M = 2.6$ Å^3 Da^{-1}, solvent content = 53%). They diffracted to around 2.0-Å resolution. For freezing, crystals were incubated for 2–5 min in a buffer containing 100 mM sodium citrate, pH 6.5, 20% PEG 4000, 0.1 M NaCl, 5% 2-propanol, and 15% glycerol.

Native data were collected at beamline ID14.4 of the European Synchrotron Radiation Facility in Grenoble, whereas MAD data were collected at the BW6 beamline of DESY in Hamburg. Data processing was performed with the HKL[56] and XDS[57] program suites. Statistics of data sets are summarized in Table 1.

Phase determination and refinement

The [4Fe–4S] clusters were found using SHELXD[58] and further refined using SHARP.[59] The phases were calculated with SHARP and improved by solvent flattening[60] assuming a solvent content of 50%. Twofold molecular averaging within DM[61] resulted in a poor electron density map that could, however, be finally interpreted using several iterative cycles of refinement and manual model building with the programs in CNS[62] and O.[63] Refinement was brought to convergence using REFMAC5.[64,65] The problem was that only one αβ heterodimer has a clearly defined electron density, which hampers the applications of solvent flattening and molecular averaging phase improvement methods. Refined thermal displacement *B*-factors are lowest for residues 56–59 and 84–90 of chain B within the rigid αβ dimer rather than near the center of gravity of the whole tetramer. There is a close correlation of the size of the *B*-values with the increasing distance from this 'cold' region. In addition, the electron density of distant atoms shows a characteristic anisotropy (extended perpendicular to the line to the cold region). This behavior is consistent with a rigid body libration of the whole tetramer that can be accounted for by the TLS (translation–libration–screw) model. Indeed, the refinement of the additional free 20 parameters (compared with the ca 43,000 of the protein model) decreases the R_{free} value by 3%. A view of the packing of the molecules in the crystal shows the 'cold' ends of the tetramers in contact to one another, related by the 21 axes. The same holds for the 'hot' ends. The R_{free} value further decreases when applying the non-crystallographic symmetry as an appropriate restraint. The refinement statistics are given in Table 1. The quality of the model was checked with PROCHECK.[66] There are four non-glycine residues in Ramachandran disallowed regions. Sequence discrepancies between the *A. fulgidus* genome[67] and the previously determined gene sequence of dSir[37] could be mostly clarified in favor of the latter. Figures 1, 2a, 3, 4 and 5 were generated with PyMOL†.

Protein Data Bank accession code

The coordinates of dSir from *A. fulgidus* are deposited in the RCSB Protein Data Bank‡ with accession number 3c7b.

Acknowledgements

This work was supported by the Max-Planck-Gesellschaft and the Deutsche Forschungsgemeinschaft (ER 222/2-1,2; PK 451/32-3). We thank the staff of the BW6 beamline (in particular, Gleb Bourenkov) at the DESY (Hamburg) as well as of the ID14.4 beamline in Grenoble for excellent technical assistance and Hartmut Michel for continuous support.

References

1. Canfield, D. E., Rosing, M. T. & Bjerrum, C. (2006). Early anaerobic metabolisms. *Philos. Trans. R. Soc. London, Ser. B*, **361**, 1819–1836.
2. Peck, H. D., Jr & Le Gall, J. (1994). Inorganic microbial sulfur metabolism. *Methods Enzymol.* **243**, 3–682.
3. Postgate, J. R. (1984). *The Sulphate Reducing Bacteria*, 2nd edit., Cambridge University Press, Cambridge, UK.
4. Odom, J. M. & Peck, H. D. (1981). Localization of dehydrogenases, reductases, and electron transfer

† http://www.pymol.org
‡ http://www.rcsb.org

components in the sulfate-reducing bacterium *Desulfovibrio gigas*. *J. Bacteriol.* **147**, 161–169.
5. Hansen, T. A. (1994). Metabolism of sulfate-reducing prokaryotes. *Antonie van Leeuwenhoek*, **66**, 165–185.
6. Fritz, G., Einsle, O., Rudolf, M., Schiffer, A. & Kroneck, P. M. H. (2005). Key bacterial multi-centered metal enzymes involved in nitrate and sulfate respiration. *J. Mol. Microbiol. Biotechnol.* **10**, 223–233.
7. Fritz, G., Schiffer, A., Behrens, A., Büchert, T., Ermler, U. & Kroneck, P. M. H. (2007). Living on sulfate: three-dimensional structure and spectroscopy of adenosine 5′-phosphosulfate reductase and dissimilatory sulfite reductase. In *Microbial Sulfur Metabolism* (Dahl, C. & Friedrich, C., eds), pp. 13–23, Springer, Berlin, Germany.
8. Thauer, R. K., Jungermann, K. & Decker, K. (1977). Energy conservation in chemotrophic anaerobic bacteria. *Bacteriol. Rev.* **41**, 100–180.
9. Hipp, W. M., Pott, A. S., Thum-Schmitz, N., Faath, I., Dahl, C. & Trüper, H. G. (1997). Towards the phylogeny of APS reductases and sirohaem sulfite reductases in sulfate-reducing and sulfur-oxidizing prokaryotes. *Microbiology*, **143**, 2891–2902.
10. Schwenn, J. D. (1997). Assimilatory reduction of inorganic sulphate. In *Sulfur Nutrition and Assimilation in Higher Plants* (Cram, J. W., ed), pp. 3–23, Academic Publishing, The Hague, The Netherlands.
11. Wirtz, M. & Droux, M. (2005). Synthesis of the sulfur amino acids: cysteine and methionine. *Photosynth. Res.* **86**, 345–362.
12. Chartron, J., Carroll, K. S., Shiau, C., Gao, H., Leary, J. A., Bertozzi, C. R. & Stout, C. D. (2006). Substrate recognition, protein dynamics, and iron–sulfur cluster in *Pseudomonas aeruginosa* adenosine 5′-phosphosulfate reductase. *J. Mol. Biol.* **364**, 152–169.
13. Crane, B. R. & Getzoff, E. D. (1996). The relationship between structure and function for the sulfite reductases. *Curr. Opin. Struct. Biol.* **6**, 744–756.
14. Dhillon, A., Goswami, S., Riley, M., Teske, A. & Sogin, M. (2005). Domain evolution and functional diversification of sulfite reductases. *Astrobiology*, **5**, 18–29.
15. Siegel, L. M., Murphy, M. J. & Kamin, H. (1973). Reduced nicotinamide adenine dinucleotide phosphate–sulfite reductase of enterobacteria: I. The *Escherichia coli* hemoflavoprotein: molecular parameters and prosthetic groups. *J. Biol. Chem.* **248**, 251–264.
16. Moura, I., LeGall, J., Lino, A. R., Peck, H. D., Fauque, G., Xavier, A. V. *et al.* (1988). Characterization of two dissimilatory sulfite reductases (desulforubidin and desulfoviridin) from sulfate-reducing bacteria. Mössbauer and EPR studies. *J. Am. Chem. Soc.* **110**, 1075–1082.
17. Carter, M. P., Tingey, J., Bobik, T. A. & Roth, J. R. (2001). The alternate electron acceptor tetrathionate supports B_{12}-dependent anaerobic growth of *Salmonella enterica* serovar Typhimurium on ethanolamine or 1,2-propanediol. *J. Bacteriol.* **183**, 2463–2475.
18. Knaff, D. B. (1996). Ferredoxin and ferredoxin-dependent enzymes. In *Oxygenic Photosynthesis: The Light Reactions* (Ort, D. R. & Yocum, C. F., eds), pp. 333–361, Kluwer Publishers, Dordrecht, The Netherlands.
19. Marritt, S. J. & Hagen, W. R. (1996). Dissimilatory sulfite reductase revisited: the desulfoviridin molecule does contain 20 iron atoms, extensively demetallated sirohaem, and an $S=9/2$ iron–sulfur cluster. *Eur. J. Biochem.* **328**, 724–727.
20. Steuber, J., Arendsen, A. F., Hagen, W. R. & Kroneck, P. M. H. (1995). Molecular properties of the dissimilatory sulfite reductase from *Desulfovibrio desulfuricans* (Essex) and comparison with the enzyme from *Desulfovibrio vulgaris* (Hildenborough). *Eur. J. Biochem.* **233**, 873–879.
21. Molitor, M., Dahl, C., Molitor, I., Schäfer, U., Speich, N., Huber, R. & Deutzmann, R. (1998). A dissimilatory sirohaem–sulfite-reductase-type protein from the hyperthermophilic archaeon *Pyrobaculum islandicum*. *Microbiology*, **144**, 529–541.
22. Dahl, C., Kredich, N. M., Deutzmann, R. & Trüper, H. G. (1993). Dissimilatory sulfite reductase from *Archaeoglobus fulgidus*: physico-chemical properties of the enzyme and cloning, sequencing and analysis of the reductase genes. *J. Gen. Microbiol.* **139**, 1817–1828.
23. Steuber, J. & Kroneck, P. M. H. (1998). Desulfoviridin, the dissimilatory sulfite reductase from *Desulfovibrio desulfuricans* (Essex)—new structural and functional aspects of the membranous enzyme. *Inorg. Chim. Acta*, **276**, 52–57.
24. Pierik, A. J. & Hagen, W. R. (1991). $S=9/2$ EPR signals are evidence against coupling between the siroheme and Fe/S cluster prosthetic groups in *Desulfovibrio vulgaris* (Hildenborough) dissimilatory sulfite reductase. *Eur. J. Biochem.* **195**, 505–516.
25. Janick, P. & Siegel, L. M. (1982). Electron paramagnetic resonance and optical spectroscopic evidence for interaction between siroheme and Fe_4S_4 prosthetic groups in *Escherichia coli* sulfite reductase hemoprotein subunit. *Biochemistry*, **21**, 3538–3574.
26. Hall, M. H., Prince, R. H. & Cammack, R. (1979). EPR spectroscopy of the iron–sulphur cluster and sirohaem in the dissimilatory sulphite reductase from *Desulfovibrio gigas*. *Biochem. Biophys. Res. Commun.* **581**, 27–33.
27. Wolfe, B. M., Lui, S. M. & Cowan, J. A. (1994). Desulfoviridin: a multimeric-dissimilatory sulfite reductase from *Desulfovibrio vulgaris* (Hildenborough). Purification, characterization, kinetics and EPR studies. *Eur. J. Biochem.* **223**, 79–89.
28. Schiffer, A. (2005). Structural and functional investigations on multi-site metalloenzymes of the biological sulfur cycle. PhD thesis, Universität Konstanz, Germany.
29. Mander, G. J., Weiss, M. S., Hedderich, R., Kahnt, J., Ermler, U. & Warkentin, E. (2005). X-ray structure of the gamma-subunit of the dissimilatory sulfite reductase: redox-active and structural disulfide bonds. *FEBS Lett.* **579**, 4600–4604.
30. Mizuno, N., Voordouw, G., Miki, K., Sarai, A. & Higuchi, Y. (2003). Crystal structure of dissimilatory sulfite reductase D (DsrD) protein—possible interaction with B- and Z-DNA by its winged-helix motif. *Structure*, **11**, 1133–1140.
31. Crane, B. R., Siegel, L. M. & Getzoff, E. D. (1995). Sulfite reductase structure at 1.6 Å: evolution and catalysis for reduction of inorganic anions. *Science*, **270**, 59–67.
32. Schnell, R., Sandalova, T., Hellman, U., Lindqvist, Y. & Schneider, G. (2005). Siroheme- and $[Fe_4S_4]$-dependent NirA from *Mycobacterium tuberculosis* is a sulfite reductase with a covalent Cys–Tyr bond in the active site. *J. Biol. Chem.* **280**, 27319–27328.
33. Swamy, U., Wang, M., Tripathy, J. M., Kim, S.-K., Hisasawa, M., Knaff, D. B. & Allen, J. P. (2005). Structure of spinach nitrite reductase: implications for multi-electron reactions by the iron–sulfur:siroheme cofactor. *Biochemistry*, **44**, 16054–16063.
34. Stetter, K. O., Lauerer, G., Thomm, M. & Neuner, A. (1987). Isolation of extreme thermophilic sulfate reducers: evidence for a novel branch of archaebacteria. *Science*, **236**, 822–824.
35. Klein, M. M., Friedrich, M., Roger, A. J., Hugenholtz, P., Fishbain, S., Abicht, H. *et al.* (2001). Multiple lateral

gene transfers of dissimilatory sulfite reductase genes between major lineages of sulfate-reducing prokaryotes. *J. Bacteriol.* **183**, 6028–6035.
36. Stahl, D. A., Fishbain, S., Klein, M., Baker, B. J. & Wagner, M. (2002). Origins and diversification of sulfate-respiring microorganisms. *Antonie van Leeuwenhoek*, **81**, 189–195.
37. Dahl, C. & Trüper, H. G. (2001). Sulfite reductase and APS reductase from *Archaeoglobus fulgidus*. *Methods Enzymol.* **331**, 427–441.
38. Holm, L. & Sander, C. (1993). Protein structure comparison by alignment of distance matrices. *J. Mol. Biol.* **233**, 123–138.
39. Hubbard, S. J., Campbell, S. F. & Thornton, J. M. (1991). Molecular recognition. Conformational analysis of limited proteolytic sites and serine proteinase protein inhibitors. *J. Mol. Biol.* **220**, 507–530.
40. Janin, J. (1997). Specific *versus* non-specific contacts in protein crystals. *Nat. Struct. Biol.* **4**, 973–974.
41. Jaenicke, R. & Bohm, G. (1998). The stability of proteins in extreme environments. *Curr. Opin. Struct. Biol.* **8**, 738–748.
42. Bornemann, S. (2002). Flavoenzymes that catalyse reactions with no net redox change. *Nat. Prod. Rep.* **19**, 761–772.
43. Siegel, L. M., Davis, P. S. & Kamin, H. (1974). Reduced nicotinamide adenine dinucleotide phosphate–sulfite reductase of enterobacteria: 3. The *Escherichia coli* hemoflavoprotein: catalytic parameters and the sequence of electron flow. *J. Biol. Chem.* **249**, 1572–1586.
44. Knaff, D. B. & Hirasawa, M. (1991). Ferredoxin-dependent chloroplast enzymes. *Biochim. Biophys. Acta*, **1056**, 93–125.
45. Fritz, G., Roth, A., Schiffer, A., Büchert, T., Bourenkov, G., Bartunik, H. D. *et al.* (2002). Crystal structure of the adenylylsulfate reductase from the hyperthermophilic archaeon *Archaeoglobus fulgidus* at 1.6 Å resolution. *Proc. Natl Acad. Sci. USA*, **99**, 1836–1841.
46. Page, C. C., Moser, C. C. & Dutton, P. L. (2003). Mechanism for electron transfer within and between proteins. *Curr. Opin. Chem. Biol.* **5**, 551–556.
47. Möller-Zinhahn, D. & Thauer, R. K. (1990). Anaerobic lactate oxidation to 3 CO_2 by *Archaeoglobus fulgidus* via the carbon monoxide dehydrogenase pathway: demonstration of the acetyl-CoA carbon–carbon cleavage reaction in cell extracts. *Arch. Microbiol.* **153**, 215–218.
48. Kunow, J., Linder, D., Stetter, K. O. & Thauer, R. K. (1994). $F_{420}H_2$: quinone oxidoreductase from *Archaeoglobus fulgidus*. Characterization of a membrane-bound multisubunit complex containing FAD and iron–sulfur clusters. *Eur. J. Biochem.* **223**, 503–511.
49. Mander, G. J., Duin, E. C., Linder, D., Stetter, K. O. & Hedderich, R. (2002). Purification and characterization of a membrane-bound enzyme complex from the sulfate-reducing archaeon *Archaeoglobus fulgidus* related to heterodisulfide reductase from methanogenic archaea. *Eur. J. Biochem.* **269**, 1895–1904.
50. Hedderich, R., Berkessel, A. & Thauer, R. K. (1989). Catalytic properties of the heterodisulfide reductase involved in the final step of methanogenesis. *FEBS Lett.* **255**, 67–71.
51. Frazao, C., Silva, G., Gomes, C. M., Matias, P., Coelho, R., Sieker, L. *et al.* (2000). Structure of a dioxygen reduction enzyme from *Desulfovibrio gigas*. *Nat. Struct. Biol.* **7**, 1041–1045.
52. Hagemeier, C. H., Krüer, M., Thauer, R. K., Warkentin, E. & Ermler, U. (2006). Insight into the mechanism of biological methanol activation based on the crystal structure of the methanol:cobalamin methyltransferase complex MtaBC. *Proc. Natl Acad. Sci. USA*, **103**, 18917–18922.
53. Lynch, M. & Conery, J. S. (2000). The evolutionary fate and consequences of duplicate genes. *Science*, **290**, 1151–1155.
54. Snel, B., Bork, P. & Huynen, M. (2000). Genome evolution. Gene fusion *versus* gene fission. *Trends Genet.* **16**, 9–11.
55. Vogel, C., Bashton, M., Kerrison, N. D., Chothia, C. & Teichmann, S. A. (2004). Structure, function and evolution of multidomain proteins. *Curr. Opin. Struct. Biol.* **14**, 208–216.
56. Otwinowski, Z. & Minor, W. (1996). Processing of X-ray diffraction data collected in oscillation mode. *Methods Enzymol.* **276**, 307–326.
57. Kabsch, W. (1993). Automatic processing of rotation diffraction data from crystals of initially unknown symmetry and cell constants. *J. Appl. Crystallogr.* **26**, 795–800.
58. Schneider, T. R. & Sheldrick, G. M. (2002). Substructure solution with SHELXD. *Acta Crystallogr., Sect. D: Biol. Crystallogr.* **58**, 1772–1779.
59. De la Fortelle, E. & Bricogne, G. (1997). Maximum-likelihood heavy-atom parameter refinement for multiple isomorphous replacement and multiwavelength anomalous diffraction methods. *Methods Enzymol.* **276**, 472–494.
60. Abrahams, J. P. & Leslie, A. G. W. (1996). Methods used in the structure determination of bovine mitochondrial F_1 ATPase. *Acta Crystallogr., Sect. D: Biol. Crystallogr.* **52**, 30–42.
61. Cowtan, K. D. (1994). 'DM': an automated procedure for phase improvement by density modification. *Joint CCP4 and ESF-EACBM Newsletter on Protein Crystallography*, **31**, 83–91.
62. Brünger, A., Adams, P. D., Clore, G. M., DeLano, W. L., Gros, P., Grosse-Kunstleve, R. W. *et al.* (1998). Crystallography & NMR System: a new software suite for macromolecular structure determinations. *Acta Crystallogr., Sect. D: Biol. Crystallogr.* **54**, 905–921.
63. Jones, T. A., Zou, J. Y., Cowan, S. W. & Kjeldgaard, M. (1991). Improved methods for building protein models in electron density maps and the location of errors in these models. *Acta Crystallogr., Sect. A: Found. Crystallogr.* **47**, 110–119.
64. Murshudov, G. N., Vagin, A. A. & Dodson, E. J. (1997). Refinement of macromolecular structures by the maximum-likelihood method. *Acta Crystallogr., Sect. D: Biol. Crystallogr.* **53**, 240–255.
65. Collaborative Computational Project, Number 4. (1994). The CCP4 Suite: programs for protein crystallography. *Acta Crystallogr., Sect. D: Biol. Crystallogr.* **50**, 760–763.
66. Laskowski, R. A., MacArthur, M. W., Moss, D. S. & Thornton, J. M. (1993). PROCHECK: a program to check the stereochemical quality of protein structures. *J. Appl. Crystallogr.* **26**, 283–291.
67. Klenk, H.-P., Clayton, R. A., Tomb, J. F., White, O., Nelson, K. E., Ketchum, K. A. *et al.* (1997). The complete genome sequence of the hyperthermophilic, sulphate-reducing archaeon *Archaeoglobus fulgidus*. *Nature*, **390**, 364–370.